

Semi-active control of vibrations of spar type floating offshore wind turbines

Van-Nguyen Dinh¹, Biswajit Basu^{*2} and Satish Nagarajaiah³

¹Software Division, Wood Group Kenny, Galway Technology Park, Parkmore, Galway, Ireland

²Department of Civil, Structural and Environmental Engineering, Trinity College Dublin, Ireland

³Departments of Civil and Environmental Engineering and Mechanical Engineering, Rice University, Houston, TX, United States

(Received March 7, 2015, Revised December 20, 2015, Accepted March 28, 2016)

Abstract. A semi-active algorithm for edgewise vibration control of the spar-type floating offshore wind turbine (SFOWT) blades, nacelle and spar platform is developed in this paper. A tuned mass damper (TMD) is placed in each blade, in the nacelle and on the spar to control the vibrations for these components. A Short Time Fourier Transform algorithm is used for semi-active control of the TMDs. The mathematical formulation of the integrated SFOWT-TMDs system is derived by using Euler-Lagrangian equations. The theoretical model derived is a time-varying system considering the aerodynamic properties of the blade, variable mass and stiffness per unit length, gravity, the interactions among the blades, nacelle, spar, mooring system and the TMDs, the hydrodynamic effects, the restoring moment and the buoyancy force. The aerodynamic loads on the nacelle and the spar due to their coupling with the blades are also considered. The effectiveness of the semi-active TMDs is investigated in the numerical examples where the mooring cable tension, rotor speed and the blade stiffness are varying over time. Except for excessively large strokes of the nacelle TMD, the semi-active algorithm is considerably more effective than the passive one in all cases and its effectiveness is restricted by the low-frequency nature of the nacelle and the spar responses.

Keywords: floating offshore wind turbine; spar-type; edgewise vibration; tuned mass damper; semi-active control

1. Introduction

Offshore wind power has great potential in near-shore deep-water zones in many countries. In deep-water areas, floating wind turbines is considered to be the most cost-effective and a reasonable solution that results in installation of larger wind turbines with capacities of 5-10 MW to minimize the power generation cost (ISSC 2009). The spar-type floating offshore wind turbine (SFOWT) seems to be a suitable concept for deep-water areas because of its lowered center of mass, small water plane area and deep-draft (Dinh and Basu 2013). An offshore floating wind turbine (FOWT) must safely withstand various environmental impacts including wind and wave loads and hydrodynamic effects and mitigation of the vibrations and the effects of such loads is extremely important for FOWTs (Lackner and Rotea 2011).

*Corresponding author, Professor, E-mail: BASUB@tcd.ie

Various measures for vibration control of FOWT blades developed for onshore wind turbines include the passive tuned mass damper (PTMD) (Murtagh *et al.* 2008) and the semi-active TMD (Arrigan *et al.* 2011, Arrigan *et al.* 2014). A pair of actuators/active tendons mounted inside each blade were proposed to control effectively the edgewise vibration of that blade (Staino *et al.* 2012). The in-plane vibrations in rotating wind turbine blades were significantly mitigated by using active TMDs (Fitzgerald *et al.* 2013). Tower responses in offshore fixed-base wind turbines could be effectively controlled by a tuned liquid column damper (TLCD) (Colwell and Basu 2009).

Different algorithms have been proposed to further improve the vibration reduction efficiency. Considering both the energy consumption and vibration reduction efficiency, STMD devices seem to be a good choice (Huang *et al.* 2010). STMD devices do not inject mechanical energy into the controlled structural system, but can be controlled to optimally reduce the system response. A Short Time Fourier Transform (STFT) algorithm to track the dominant frequency of the system over time was introduced (Nagarajaiah and Varadarajan 2005). In that algorithm, the structures response was split into segments and each segment was analysed in real-time by performing a Fast Fourier Transform (FFT) to identify the current dominant frequency in the system. That algorithm enabled their STMD to be continuously tuned to the dominant frequency of the structure resulting in a significantly improved response than that achieved by a conventional passive TMD. The STFT technique has been effectively applied into various structures (Nagarajaiah and Sonmez 2007, Nagarajaiah 2009).

In controlling FOWTs, the blade pitch angle and the generator torque approaches suffer from some critical drawbacks (Lackner 2009), and so the structural control approaches may be suitable alternatives. In this paper, a TMD is therefore placed in each blade, in the nacelle and on the spar platform to control the vibrations of these components and the STFT algorithm is used for semi-active control. The controlled mathematical model of the integrated SFOWT-TMDs system is developed using the Euler-Lagrangian energy formulation. The edgewise vibrations are the focus as they are known to be lightly damped and can lead to violent vibrations; the first edgewise mode may exhibit a very low or even negative damping under certain conditions.

The developed SFOWT-TMDs model in this paper is a time-varying MDOF system considering the aerodynamic properties of the blade, variable mass and stiffness per unit length, gravity, the interactions among the blades, nacelle, spar, mooring system and the TMDs, the hydrodynamic effects, the restoring moment and the buoyancy force. The aerodynamic loads on the nacelle and the spar due to their coupling with the blades are also considered. The ocean wave model and the uncontrolled SFOWT model developed and validated by Dinh *et al.* (2013), and parameters resulting from passive control of SFOWT spar motions by using TMDs (Dinh and Basu 2014) are utilized. The effectiveness of the STMD strategy and the STFT algorithm is investigated in three numerical examples. In the first two examples, the varying tension of mooring cables and the varying rotational speed of the blades are considered, respectively. In the last example, the stiffness of a blade, the tension of mooring cables and the rotor speed are all varying.

2. Theoretical model formulation of SFOWT-TMD system

In the model proposed in this paper, the spar is assumed to be a rigid body due to its large cross section. The displacement and velocity of the FOWT system are assumed to be small. As the spar diameter is small compared to its draft and to the wavelength, Morison's equation can be used to

calculate the hydrodynamic loads. The mooring cables are assumed to be perfectly flexible, inextensible, and heavy so that the extended quasi-static model of mooring cable developed by Sannasiraj *et al.* (1998) for moored floating breakwaters can be adopted. A TMD is embedded into each blade in order to reduce the edgewise vibration. A TMD is also installed into the nacelle and the spar, respectively. All the TMDs are modelled as single degree of freedom (SDOF) systems.

The proposed coupled model of a three-bladed horizontal-axis SFOWT-TMD is shown in Fig. 1 and the definitions of other model parameters are given in Table 1. The coupled model aims at representing the edgewise vibration responses and the associated coupling of the blades with the motions of the tower/nacelle and the spar. In this model, the blades are modeled as Bernoulli–Euler cantilever beams of length ‘ R ’, with variable bending stiffness and variable mass per unit length $\mu(r)$ along the length as shown in Fig. 2. The blades rotate at a speed Ω (rad/s) and the azimuthal angle $\Psi_i(t)$ of blade ‘ i ’ at the time instant ‘ t ’ is expressed as

$$\Psi_i(t) = \Psi_1(t) + (i-1)\frac{2\pi}{3}, \quad \Psi_1(t) = \Omega t, \quad i = 1, 2, 3 \tag{1}$$

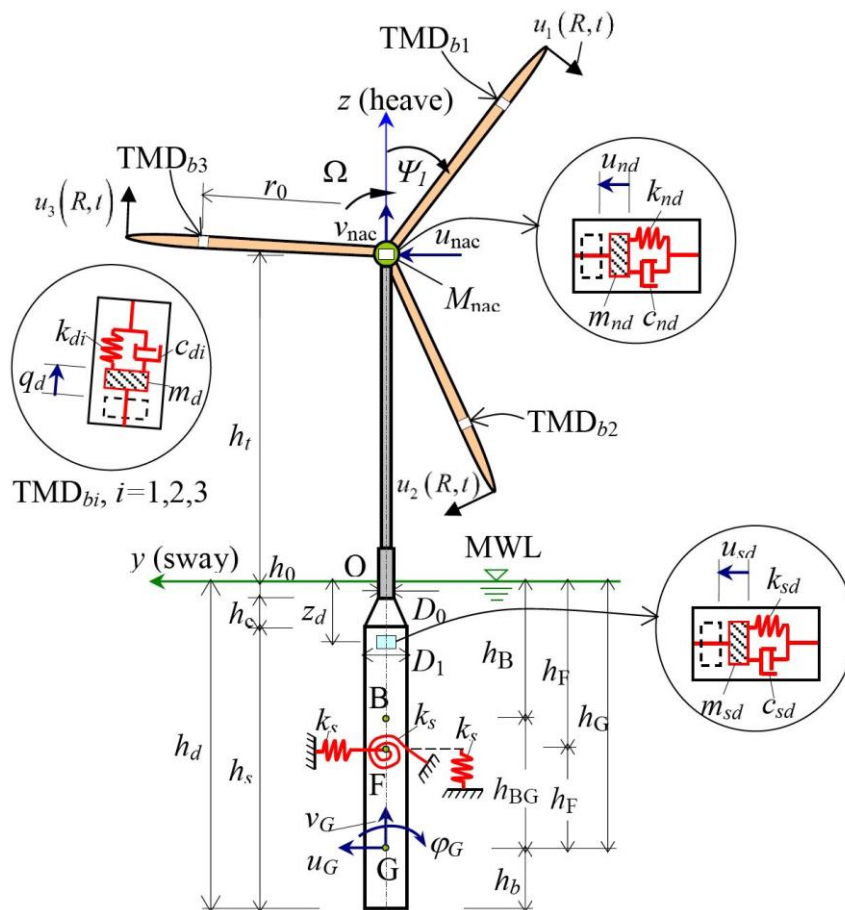
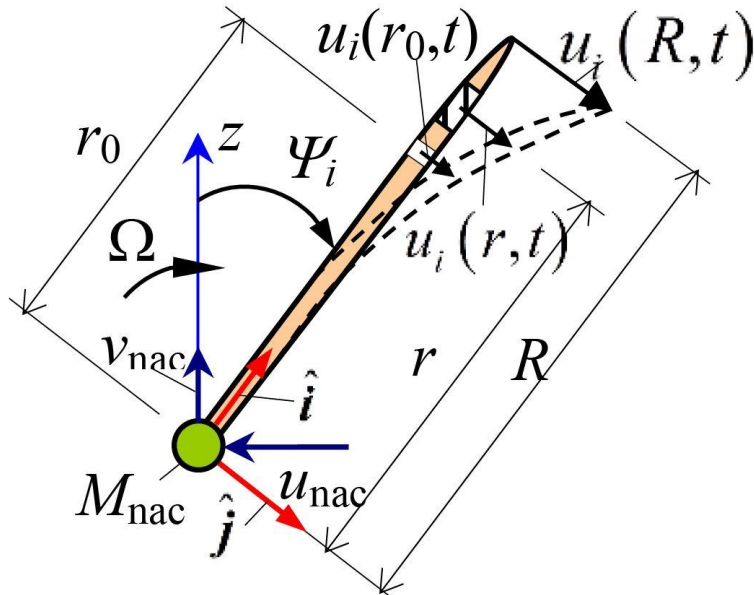


Fig. 1 Edgewise coupled model of SFOWT-TMDs system and parameters

Table 1 Notations for edge-wise model of SFOWT-TMDs

B = Center of buoyancy of the S-FOWT.	h_F = Depth of fairleads F.
G = Center of gravity of the S-FOWT.	r_0 = location of damper along the blade
F = Fairlead position at spar centreline.	d_0 = Offset position of damper from centreline of the blade.
Oyz = Global axes, O at mean water level (MWL)	z_d = Depth of spar TMD below MWL.
u_G, v_G, φ_G = Absolute sway, heave and roll displacement at G.	θ_0 = Angle at the anchor points C_l and C_r
$k_{sH}, k_{sV}, k_{s\varphi}$ = Horizontal, vertical and roll stiffness of mooring system, respectively.	C', C = Imaginary anchor and real anchor.
M_c = Mass of each mooring cable in water.	T_0 = Initial horizontal tension of each mooring cable.
M_0 = Mass of nacelle + modal mass of tower	ρ_c = Cable mass per unit length.
D_0 = Diameter of spar above taper.	w = Weight per unit length of mooring line in water
D_1 = Diameter of spar below taper.	l = Imaginary extension length to make a zero contact angle
M_s = Mass of the spar.	$Z_{FC'}, Z_{FC}$ = Vertical distance between F and C' and C.
M_s, I_s = Moment of inertia of the spar.	L = Real length of cable.
h_t = Tower top (yaw bearing) above MWL	$L' = L + l$ = Total length of cable.
h_0 = Depth to top of taper below MWL.	$Y_{FC'}, Y_{FC}$ = Horizontal distances between F and C' and C.
h_c = Height of spar taper	y_F, y_G = Horizontal coordinates of F and G in Oyz axes.
h_s = Height of spar cylinder (from taper bottom to spar bottom).	z_F, z_G = Vertical coordinates of F and G in Oyz axes,
h_d = Depth to spar bottom below MWL.	T_C, T_F = Initial cable tensions at C and F.
h_G = Depth of G below MWL.	
h_B = Depth of B below MWL.	

Fig. 2 Geometry of blade i and its TMD

For simplification in modelling and practical installation, the blade TMDs are assumed to have the same distance r_0 from the hub, the same mass ($m_{d1} = m_{d2} = m_{d3} = m_d$) and the same damping ratio ($\zeta_{d1} = \zeta_{d2} = \zeta_{d3} = \zeta_d$) but variable stiffness (k_{di} , $i = 1, 2, 3$). The constant mass and damping ratio and the varying stiffness of the nacelle TMD are m_{nd} , ζ_{nd} and k_{nd} , respectively. The mass, damping ratio and stiffness of the spar TMD are m_{sd} , ζ_{sd} and k_{sd} , respectively. Real-time tuning frequencies of the blade TMDs $\omega_{di}(t)$, ($i = 1, 2, 3$), the nacelle TMD $\omega_{nd}(t)$, and the spar TMD $\omega_{sd}(t)$ are provided by the semi-active control scheme presented in the next section. The time-varying damping coefficients and stiffness of the blade TMDs, nacelle TMD and spar TMD are respectively expressed as

$$c_{di}(t) = 2m_d\omega_{di}(t)\zeta_d; \quad k_{di}(t) = 2m_d\omega_{di}^2(t) \quad (2a)$$

$$c_{nd}(t) = 2m_{nd}\omega_{nd}(t)\zeta_{nd}; \quad k_{nd}(t) = 2m_{nd}\omega_{nd}^2(t) \quad (2b)$$

$$c_{sd}(t) = 2m_{sd}\omega_{sd}(t)\zeta_{sd}; \quad k_{sd}(t) = 2m_{sd}\omega_{sd}^2(t) \quad (2c)$$

Only the fundamental edgewise modes of the blades are considered in this paper. The tower is modeled as a single degree of freedom (SDOF) system with the generalized stiffness k_t . As the axial deformations of the spar and the tower are neglected, and the roll displacement of the spar φ_G is small, the absolute vertical displacement of the nacelle is approximated as

$$\bar{v}_{nac} = v_G - h_a(1 - \cos\varphi_G) \approx v_G \quad (3)$$

The absolute horizontal displacement \bar{u}_{nac} of the nacelle is approximated as

$$\bar{u}_{nac} \approx u_{nac} + u_G - h_a\varphi_G \quad (4)$$

where h_a is the vertical distance between the tower top and the center of gravity, $h_a = h_t + h_G$.

The vector of generalized coordinates of the SFOWT-TMDs system is

$$\mathbf{q}(t) = \langle q_1 \quad q_{d1} \quad q_2 \quad q_{d2} \quad q_3 \quad q_{d3} \quad u_{nac} \quad u_G \quad v_G \quad \varphi_G \quad u_{nd} \quad u_{sd} \rangle^T \quad (5)$$

where the degree of freedom q_i , $i = 1, 2, 3$ relates to the fundamental edgewise mode of the blade “ i ”. The relative displacement of the TMD in the i th blade with respect to the blade is denoted as q_{di} . The edgewise displacement along the blade i can be approximated by using its fundamental edgewise mode shape $\phi_1(r)$ as $u_i(r, t) = \phi_1(r)q_i(t)$. The variable $u_{nac}(t)$ represents the relative sway displacement of the nacelle with respect to the spar sway displacement u_G . The term v_G is the spar heave displacement. The terms u_{nd} and u_{sd} are the relative displacements of the nacelle TMD and the spar TMD with respect to the nacelle and the spar, respectively.

From Fig. 2, the absolute velocity vector of a point r on the blade i at a time t is written as

$$\mathbf{v}_{bi}(r, t) = \left[-\dot{\bar{u}}_{nac} \sin\psi_i + \dot{\bar{v}}_{nac} \cos\psi_i - \Omega u_i(r, t) \right] \hat{\mathbf{i}} + \left[-\dot{\bar{u}}_{nac} \cos\psi_i - \dot{\bar{v}}_{nac} \sin\psi_i + \dot{u}_i(r, t) + \Omega r \right] \hat{\mathbf{j}} \quad (6)$$

where $\hat{\mathbf{i}}$ and $\hat{\mathbf{j}}$ are the unit vectors along and perpendicular to the blade center line, respectively. The absolute velocity vector of the damper in blade i at time t is expressed as

$$\mathbf{v}_{di}(t) = \left[-\dot{u}_{nac} \sin \psi_i + \dot{v}_{nac} \cos \psi_i - \Omega u_i(r_0, t) - \Omega q_{di} - \Omega d_0 \right] \hat{\mathbf{i}} + \left[-\dot{u}_{nac} \cos \psi_i - \dot{v}_{nac} \sin \psi_i + \dot{u}_i(r_0, t) + \dot{q}_{di} + \Omega r_0 \right] \hat{\mathbf{j}} \tag{7}$$

The total kinetic energy of the whole SFOWT-TMDs system is expressed as

$$T = \frac{1}{2} \sum_{i=1}^3 \int \mu(r) |\mathbf{v}_{bi}|^2(r, t) dr + \frac{1}{2} m_d \sum_{i=1}^3 \mathbf{v}_{di}^2(t) + \frac{1}{2} M_{nac} (\dot{u}_{nac}^2 + \dot{v}_{nac}^2) + \frac{1}{2} m_{nd} (\dot{u}_{nac} + \dot{u}_{nd})^2 + \frac{1}{2} M_s (\dot{u}_G^2 + \dot{v}_G^2) + \frac{1}{2} I_s \dot{\phi}_G^2 + \frac{1}{2} m_{sd} (\dot{u}_s + \dot{u}_{sd})^2 \tag{8}$$

The total potential energy of whole SFOWT-TMDs system is expressed as

$$V = \frac{1}{2} \sum_{i=1}^3 (K_e + K_w \cos \psi_i + K_g) d_i^2 + \frac{1}{2} \sum_{i=1}^3 k_{di} q_{di}^2 + \frac{1}{2} k_t \bar{u}_{nac}^2 + \frac{1}{2} k_{nd} u_{nd}^2 + \frac{1}{2} k_{sH} u_G^2 + \frac{1}{2} k_{sV} v_G^2 + \frac{1}{2} k_{s\phi} \phi_G^2 + \frac{1}{2} k_{sd} u_{sd}^2 \tag{9}$$

where the parameter K_e is the generalized elastic stiffness of the blade, $K_e = \omega_b^2 m_2$ with ω_b as the fundamental natural frequency of the blade and m_2 as the modal mass of the blade. The term K_w is the stiffness arising out of gravity effects, $K_w = -g \int_0^R \int_r^R \mu(\xi) d\xi [\phi_1']^2 dr$. The term $K_g = \Omega^2 K_{g,0}$ is the geometrical stiffness due to centrifugal force on blade in which $K_{g,0} = \int_0^R \int_r^R \mu(\xi) \xi d\xi [\phi_1']^2 dr$ (Staino *et al* 2012, Basu *et al* 2012). Assuming that the spar roll displacement ϕ_G is small, the spar horizontal displacement u_s at the depth z_d is approximated as

$$u_s = u_s(z_d) \approx u_G - (z_d + h_G) \phi_G \tag{10}$$

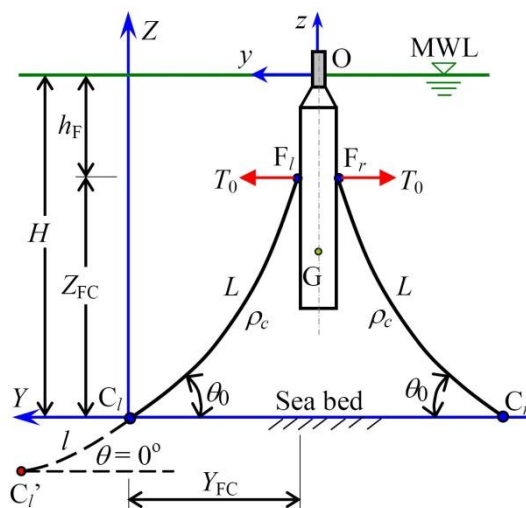


Fig. 3 Mooring model

Substituting expressions of the system kinetic energy in Eq. (8) and potential energy in Eq. (9) into the Euler-Lagrange equations in Eq. (11)

$$\frac{d}{dt} \left(\frac{\partial T}{\partial \dot{\mathbf{q}}} \right) - \frac{\partial T}{\partial \mathbf{q}} + \frac{\partial V}{\partial \mathbf{q}} = \mathbf{Q}_{\text{ext}} \quad (11)$$

the aerodynamic and structural portions of the mass, damping and stiffness matrices of the SFOWT-TMDs system can be obtained and are expressed in Appendix A. The relative velocities and damping of the TMDs also add dissipative forces (non-conservative) to the system. D' Alembert's equation is used to find the additional terms to the system damping matrix.

The parameters of the mooring system are shown in Fig. 3 and Table 1 and the initial horizontal tension T_0 is assumed to be constant along the cable length.

3. Modelling of loads

The wind load, gravitational load, hydrostatic load and hydrodynamic effects that excite the floating offshore wind turbines are presented in the following sections.

3.1 Aerodynamic load

The wind load acting on the tower is neglected as it is small compared to the load on the rotor. The generalized aerodynamic load vector is obtained by differentiating the virtual work done due to the wind load acting on the SFOWT system derived by Dinh and Basu (2014) and written as

$$\mathbf{Q}_w(t) = \langle Q_{b1}^w \ 0 \ Q_{b2}^w \ 0 \ Q_{b3}^w \ 0 \ Q_{\text{coup}}^w \ Q_{\text{coup}}^w \ \bar{Q}_{\text{coup}}^w \ -h_G Q_{\text{coup}}^w \ 0 \ 0 \rangle^T \quad (12)$$

The resultant aerodynamic load on blade i , and the aerodynamic loads coupling the blade edgewise vibrations with the tower/spar sway and heave motions are respectively given as

$$Q_{b1}^w(t) = \int_0^R p_i(r,t) \phi_1(r) dr, \quad i = 1, 2, 3 \quad (13)$$

$$Q_{\text{coup}}^w = -\sum_{i=1}^3 \int_0^R p_i(r,t) dr \cos \psi_i \quad (14)$$

$$\bar{Q}_{\text{coup}}^w = -\sum_{i=1}^3 \int_0^R p_i(r,t) dr \sin \psi_i \quad (15)$$

where the variable wind load intensity along the blade length in the edgewise direction, $p_i(r,t)$ ($i = 1, 2, 3$) is calculated by using BEM theory (Hansen 2003, Staino *et al.* 2012).

3.2 Gravitational load

Differentiating the virtual work done due to the gravity (Dinh and Basu 2014) with respect to the generalized coordinates, the generalized gravitational loads on blade i and on the spar are obtained and are respectively expressed as

$$Q_{b_i}^g(t) = gm_i \sin \psi_i, \quad i = 1, 2, 3 \quad (16)$$

$$Q_{v_G}^g(t) = -g \left[\sum_{i=1}^3 \int_0^R \mu(r) dr \sin^2 \psi_i + M_0 + M_s \right] \quad (17)$$

3.3 Hydrostatic and restoring loads

The magnitude of the buoyancy force and the vertical restoring coefficient acting on the spar are respectively expressed as

$$F_{\text{buoy}} = \rho_w g V_s \quad (18)$$

$$K_V^{\text{res}} = \rho_w g A_{s_0} \quad (19)$$

where V_s is the volume of the water displaced by the spar and $A_{s_0} = \pi D_0^2/4$ is the plane water area.

The roll restoring coefficient is computed as

$$K_\phi^{\text{res}} = \left[(h_B - h_G) V_s + \frac{\pi D_0^2}{64} \right] \rho_w g \quad (20)$$

where h_B is the downward distance from the MWL to the center of buoyancy (assuming that the spar center of buoyancy B is always above its center of gravity G)

$$h_B = h_G - \overline{BG} \quad (21)$$

in which \overline{BG} is the vertical distance between the spar center of buoyancy B and center of gravity G (Dinh *et al.* 2013, Dinh and Basu 2014).

Before using Eqs. (18)-(21), the static depth h_0 of the taper top below the MWL must be re-calculated by using Archimedes's principle where the total weight of the wind turbine, spar and mooring cables in water is made equal to the weight of the water volume displaced by the spar (Dinh and Basu 2014). If the system mass is considerably increased when the TMDs are installed, h_0 and the related depths such as h_d , h_F and h_G should be re-evaluated.

3.4 Hydrodynamic effects

Hydrodynamics of FOWTs and their mooring systems were successfully modelled by using computational software (Flexcom 2015). In this paper, the hydrodynamic effects on the spar are calculated by using Morison's equation as its diameter is small relative to the wavelength. These effects consist of (i) the added mass effects associated with spar acceleration \ddot{u}_s , (ii) the inertia forces associated with fluid acceleration, and (iii) the viscous drag forces due to the squared relative velocity of the spar to the fluid. The spar roll velocity is assumed to be small. To account for depth-dependence, the strip theory is used where the draft h_d is divided into N_z depth intervals Δz_i (Dinh and Basu 2014).

The added mass coefficients in sway motion due to sway acceleration a_{yy} and in sway motion due to roll acceleration $a_{\phi\phi}$, and the added mass roll moment due to spar roll acceleration $a_{\phi\phi}$ are expressed respectively as

$$a_{yy} = C_M \rho_w \frac{\pi}{4} \sum_{i=1}^{N_z} D^2(z_i) \Delta z_i \quad (22)$$

$$a_{y\varphi} = a_{\varphi y} = -C_M \rho_w \frac{\pi}{4} \sum_{i=1}^{N_z} D^2(z_i) (z_i + h_G) \Delta z_i \quad (23)$$

$$a_{\varphi\varphi} = C_M \rho_w \frac{\pi}{4} \sum_{i=1}^{N_z} D^2(z_i) (z_i + h_G)^2 \Delta z_i \quad (24)$$

In Eqs. (22)-(24), C_M is the added mass coefficient, $C_M = 1.0$ for circular cylinder (Faltinsen 1990) and $D(z_i)$ is the spar diameter at a discrete depth z_i . Using the assumption that the volume of the added water under the spar is a half sphere (Waris and Ishihara 2012), the vertical added mass coefficient at the base of the spar is expressed as

$$a_{zz} = \rho_w \frac{\pi D_1^3}{12} \quad (25)$$

The vertical inertia force due to vertical acceleration $\ddot{v}_f(z = -h_d, t)$ of fluid particles at the spar bottom and the total horizontal inertia fluid force acting on the spar are respectively expressed as

$$F_z^f(t) = (C_M + 1) \rho_w A_{sl} \ddot{v}_f(z = -h_d, t) \quad (26)$$

$$F_y^f(t) = (C_M + 1) \rho_w \frac{\pi}{4} \sum_{i=1}^{N_z} D^2(z_i) \Delta z_i \ddot{u}_f(z_i, t) \quad (27)$$

where $\ddot{u}_f(z_i, t)$ is the horizontal acceleration of fluid particles at depth z_i and $A_{sl} = \pi D_1^2/4$.

The viscous drag forces result from the relative velocities of the spar and the fluid and exist regardless of the presence of the waves. The vertical drag force normal to the spar bottom due to its heave velocity and the total horizontal drag force are respectively expressed as

$$F_z^{Df} = \frac{1}{2} C_D^z \rho_w A_{sl} \left| \dot{\mathbf{q}}_{sf}^n(-h_d, t) \right| \left[\dot{v}_f(-h_d, t) - \dot{v}_G \right] \quad (28)$$

$$F_y^{Df} = \frac{1}{2} C_D^y \rho_w \sum_{i=1}^{N_z} D(z_i) \left| \dot{\mathbf{q}}_{sf}^n(z_i, t) \right| \left[\dot{u}_f(z_i, t) - \dot{u}_G + \dot{\phi}_G(z_i + h_G) \right] \Delta z_i \quad (29)$$

where C_D^z is the drag coefficient of heave motion and C_D^y is the hydrodynamic viscous drag coefficient of spar sides, $C_D^y = 0.6$ for cylindrical object (Waris and Ishihara 2012). The quantity $\left| \dot{\mathbf{q}}_{sf}^n(z_i, t) \right|$ is the amplitude of the relative normal velocity vector and expressed as

$$\left| \dot{\mathbf{q}}_{sf}^n(z, t) \right| = \sqrt{\left[\dot{u}_f(z, t) - \dot{u}_G + \dot{\phi}_G(z + h_G) \right]^2 + \left[\dot{v}_f(z, t) - \dot{v}_G \right]^2} \quad (30)$$

in which $\dot{u}_f(z, t)$ and $\dot{v}_f(z, t)$ are the fluid horizontal and vertical velocity, respectively.

Based on the total drag forces in Eqs. (28) and (29), the hydrodynamic damping coefficients in sway, heave and sway-roll coupling directions are defined respectively as

$$C_{uu_G}^{\text{drag}} = \frac{1}{2} C_D^y \rho_w \sum_{i=1}^{N_z} D(z_i) \Delta z_i \left| \dot{\mathbf{q}}_{sf}^n(z_i, t) \right| \quad (31)$$

$$C_{u\varphi_G}^{\text{drag}} = -\frac{1}{2} C_D^y \rho_w \sum_{i=1}^{N_z} D(z_i) (z_i + h_G) \Delta z_i \left| \dot{\mathbf{q}}_{sf}^n(z_i, t) \right| \quad (32)$$

$$C_{vv_G}^{\text{drag}}(t) = \frac{1}{2} C_D^z \rho_w A_{sl} \left| \dot{\mathbf{q}}_{sf}^n(-h_d, t) \right| \quad (33)$$

The drag loads in the sway and heave directions are defined respectively as

$$F_y^D = \frac{1}{2} C_D^y \rho_w \sum_{i=1}^{N_z} D(z_i) \Delta z_i \left| \dot{\mathbf{q}}_{sf}^n(z_i, t) \right| \dot{u}_f(z_i, t) \quad (34)$$

$$F_z^D = \frac{1}{2} C_D^z \rho_w A_{sl} \left| \dot{\mathbf{q}}_{sf}^n(-h_d, t) \right| \dot{v}_f(-h_d, t) \quad (35)$$

The horizontal and vertical velocity (in the drag force terms, Eqs. (28)-(33)) and the horizontal and vertical acceleration (in the inertia force terms, Eqs. (26) and (27)) of fluid particles at a depth of z (origin at the MWL and positive upward) and horizontal position y are given by

$$\dot{u}_f(y, z, t) = \sum_{j=1}^{N_\omega} \omega_j A_j \frac{\cosh k_j(z+H)}{\sinh k_j H} \sin \theta_j(y, t) \quad (36)$$

$$\dot{v}_f(y, z, t) = \sum_{j=1}^{N_\omega} \omega_j A_j \frac{\sinh k_j(z+H)}{\sinh k_j H} \sin \theta_j(y, t) \quad (37)$$

$$\ddot{u}_f(y, z, t) = \sum_{j=1}^{N_\omega} \omega_j^2 A_j \frac{\cosh k_j(z+H)}{\sinh k_j H} \sin \theta_j(y, t) \quad (38)$$

$$\ddot{v}_f(y, z, t) = -\sum_{j=1}^{N_\omega} \omega_j^2 A_j \frac{\sinh k_j(z+H)}{\sinh k_j H} \sin \theta_j(y, t) \quad (39)$$

respectively. In Eqs. (36)-(39), ω_j , k_j and ε_j are the circular frequency, wave number and random phase angle of wave component number j , respectively. The random phase angles ε_j are uniformly distributed between 0 and 2π . The parameters ω_j and k_j are related by the exact linear dispersion relationship $k_j \tanh(k_j H) = \omega_j^2 / g$ for any water depth H (Sarpkaya and Isaacson 1981). The wave amplitude A_j can be obtained from a wave spectrum $S(\omega)$ as

$$A_j = \sqrt{2S(\omega_j) \Delta\omega} \quad (40)$$

in which $\Delta\omega$ is the difference between successive frequencies. The Pierson-Moskowitz (PM) wave spectrum (IEC 2006) is used in this paper and its one-sided spectrum has a form

$$S(\omega) = \frac{1}{2\pi} \frac{5}{16} H_{sw}^2 T_{pw} c_{\omega}^{-5} \exp\left(-\frac{5}{4} c_{\omega}^{-4}\right) \quad (41)$$

where $c_{\omega} = \omega T_{pw} / (2\pi)$, H_{sw} is the significant wave height and T_{pw} is the spectral period; their unit must be meter and second, respectively.

4. Semi-active control strategy

In this paper, the stiffness of the TMD spring is changed according to the instant dominant frequency of the responses and the Short Time Fourier Transform (STFT) is used to evaluate that dominant frequency. For the continuous-time case, STFT is the Fourier transform of the signal multiplied with a window function which is nonzero for only a short period of time. The Fourier transform of the resulting signal is taken as the window is sliding along the time axis, resulting in a two-dimensional representation of the signal. Mathematically, this is written as

$$STFT\{x(t)\} \equiv X(\tau, \omega) = \int_{-\infty}^{\infty} x(t) w(t-\tau) e^{-j\omega t} dt \quad (42)$$

where $w(t)$ is the window function, commonly a zero mean Hanning window or Gaussian, and $x(t)$ is the signal to be transformed. The Hanning window is used in the simulation. The flowchart of the STMD strategy is shown in Fig. 4 which is expanded from the strategy by Huang *et al.* (2010). The frequency selection process is to make sure the frequency change for STMD is gradual. The procedure starts by selecting a STFT window and a window length. The response signal is convoluted with a window function and then zero padded for the desired frequency resolution. The FFT power spectrum of each window is calculated and the dominant frequency of the response $f_{inst}(t)$ at an instant of time t is determined by weighting the frequencies within the window by its normalized power spectrum value at the corresponding time. If the dominant frequency is within the lower and upper bounds, the STMD is tuned to the dominant frequency. If it is not within the bounds, STMD is tuned to the optimum passive TMD frequency. For the blades, the upper and lower bounds are defined as the limits around the blade natural frequency f_b with a deviation of 0.4Hz (as a soft constraint) on either side for the examples used in this paper.

$$f_{lim,lower}^b = (f_b - 0.4) / \Delta f \quad (43)$$

$$f_{lim,upper}^b = (f_b + 0.4) / \Delta f \quad (44)$$

where Δf is the frequency step. For the nacelle and the spar, the upper and lower bounds are defined as

$$f_{lim,upper}^b = (f_b + 0.4) / \Delta f \quad (45)$$

$$f_{lim,upper}^{n,s} = f_{TMD,prev} \left(1 + f_{rat}^{n,s}\right) \quad (46)$$

where $f_{TMD,prev}$ is the frequency of the TMD computed in the previous time step. In the examples

used in this paper $f_{rat}^n = 0.05$ for nacelle and $f_{rat}^s = 0.01$ for spar because the lower dominant frequencies of nacelle and spar responses are generally very low and even lower than 0.1 Hz.

A computer program in MATLAB environment (MATLAB 2011) for the mathematical models of the SFOWT-TMDs and the semi-active control strategy are developed in this paper. The computer programs for the wave model and the uncontrolled SFOWT model developed and validated by Dinh *et al.* (2013) are used in this paper.

5. Numerical examples

The properties of the floating platform, mooring systems and tower of the OC3 SFOWT (Jonkman 2010) are used in the numerical examples where $h_t = 87.6$ m, $h_0 = 4$ m, $h_c = 8$ m, $h_d = 120$ m, $h_F = 70$ m, $h_G = 89.9155$ m, $D_0 = 6.5$ m, $D_1 = 9.4$ m, $M_s = 7466.33 \times 10^3$ kg, $I_s = 4229.23 \times 10^6$ kg.m², $L = 902.2$ m, $\rho_c = 77.7066$ kg/m, $\theta_0 = 0^\circ$, $T_0 = 10^8$ N, $\rho_w = 1025$ kg/m³ and $H = 320$ m.

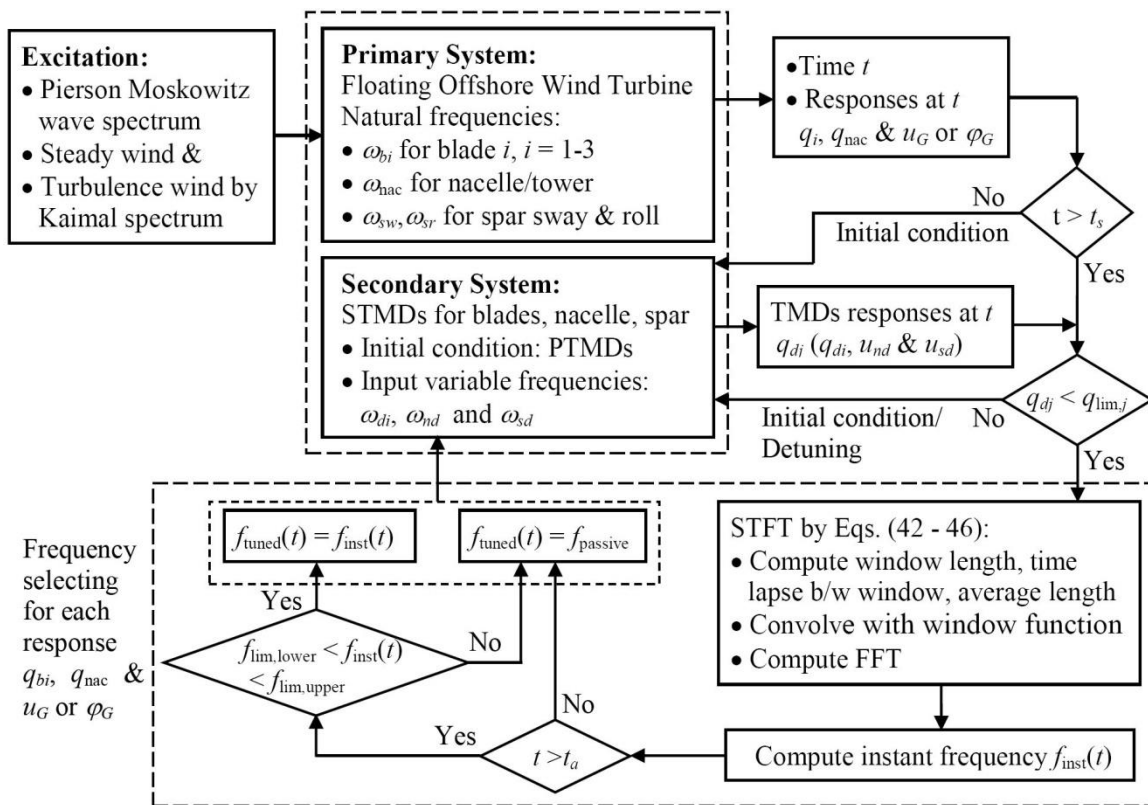


Fig. 4 Flowchart of STMD strategy

The aerodynamic, blade, hub and nacelle properties of the NREL 5-MW baseline HAWT (Jonkman *et al.* 2009) are used where $R = 61.5$ m, the cut-in and rated rotor speeds are 6.9 rpm and 12.1 rpm, respectively. The mass of each blade, hub mass, nacelle mass, and tower integrated mass are 17.74×10^3 kg, 56.78×10^3 kg, 240×10^3 kg, and 249.718×10^3 kg, respectively. The fundamental frequencies of the blade and the tower are 6.81 rad/s and 2.87 rad/s, respectively. The modal structural damping ratios of the blade and the tower are taken as 0.48% and 1%, respectively (Jonkman *et al.* 2009). The drag coefficient of heave motion $C_D^z = 2$ is assumed for the externally-smooth cylindrical spar. The values of h_0 and h_B of the controlled system with various values of the TMD mass ratios μ_{nd} and μ_{sd} have been re-evaluated by Dinh and Basu (2014); when $\mu_{sd} = 0.03$ or larger the spar would sink by 7.6 m or more due to the additional weight of the TMDs.

The wind and wave states at the operating condition are used where the mean wind speed at the top of the tower is assumed to be at the rated wind speed as 12 m/s and the turbulence intensity is 15%. The significant wave height H_{sw} of 3 m, the wave peak period T_{pw} of 10 s and the depth interval Δz of 4 m are used to simulate the sea profiles. The total simulation time and the time step interval and the frequency interval are 200 s and 0.01 s respectively.

The parameters and results from passive control of SFOWT spar motions by TMDs (Dinh and Basu 2014) are utilized in this paper. The spar TMD is located at the mean water level and its mass ratio m_{sd} is 3%. The stroke constraints for the spar TMD are 80% of the radius of its cross section ($\pm 0.8 \times 0.5 \times D_1 = \pm 3.75$ m). The control is most effective for nacelle sway and spar roll for all values of tuning frequency ω_s and an initial tension T_0 . The spar TMD is tuned at the wave peak frequency $\omega_{pw} = 0.5969$ rad/s at which the passive TMD is most effective, especially for nacelle sway and spar roll. The initial tension of mooring cable T_0 is 10^8 N. The mass ratios of the nacelle TMD and the blade TMDs are $m_{nd} = 0.01$ and $m_{bd} = 0.01$ respectively.

The stroke constraints for the blade TMDs and nacelle TMD are 80% of the blade half chord ($\pm 0.8 \times 0.5 \times 3.0 = \pm 1.2$ m) and 80% of the nacelle half width ($\pm 0.8 \times 0.5 \times 5.0 = \pm 2.0$ m), respectively. Initially, the semi-active control scheme is introduced into all TMDs in the three blades, the nacelle and the spar. However, these results in excessively large strokes of nacelle TMD and instability may occur when the TMD is tuned at low frequency. Thus, the control scheme of the nacelle TMD is passive. In order to investigate the effectiveness of the STMD strategy, three numerical examples are considered in the following sections: (i) Varying tension of mooring cables T_0 , (ii) Varying rotational speed Ω and (iii) Stiffness of a blade, tension of mooring cables and rotational speed are varying. Notes on Fourier Transform of time history data (Dinh and Basu 2012) are considered to improve the accuracy. In the STFT algorithm, the window size is defined as $50.00 + \Delta t$ and the segment length is defined as round $[(\text{window size} - \Delta t)/\Delta t]$.

5.1 Varying tension of mooring cables

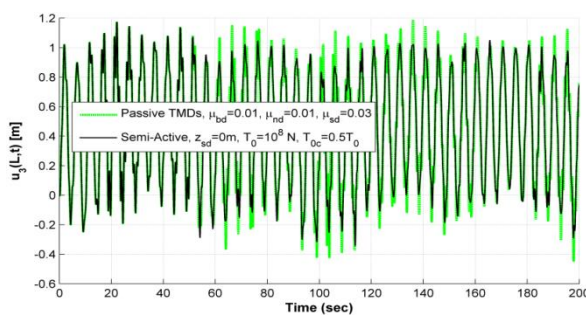
The tensions in all three mooring cables are assumed to be suddenly dropped from $T_0 = 10^8$ N to $T_{0c} = 0.5T_0$ at a time $t_1 = 80$ s. It should be noted here that the tensions in three cables must be equal to ensure stability of the SFOWT. The time histories and Fourier amplitude spectra of the blade 3 displacement, nacelle sway and spar roll controlled by passive and semi-active TMDs are shown in Figs. 5(a)-5(f), respectively where the semi-active scheme are considerably more effective than passive scheme, especially since the time $t_1 = 80$ s. This is because at the time instant $t_1 = 80$ s the cable tensions drop by one half, the spar sway and roll stiffnesses are consequently reduced and the

dominant frequencies of their motions are lowered. Thus the selection of control frequency for the passive TMD scheme is less accurate and consequently its effectiveness is reduced. Whereas for the STMD, the controlled frequency is re-tuned continuously in real-time and hence is still more accurate

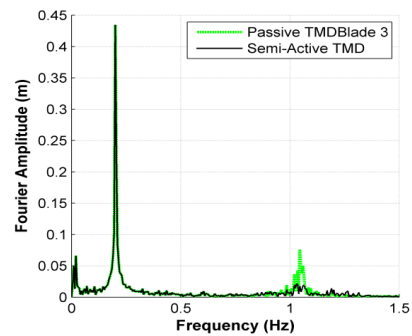
Fig. 5(h) presents the real-time frequency of the spar TMD resulted from the semi-active control. The strokes of the spar TMD shown in Fig. 5(g) vary between (-2 m, +2.5 m) that is acceptable to the spar diameter.

5.2 Varying rotational speed Ω

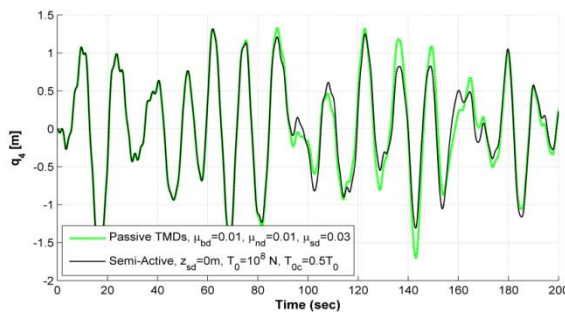
The rotor rotational speed Ω is assumed to be steeply reduced to 0.6Ω at a time $t_2 = 100$ s. The time histories and Fourier amplitude spectra of the blade 3 displacement, nacelle sway and spar roll controlled by passive and semi-active TMDs are shown in Figs. 6(a)-6(f), respectively. The effectiveness of the semi-active control on all blade displacements, nacelle sway and spar roll are larger compared with the case or varying cable tensions in Section 5.1. That difference may be due to the cable tension changes result in low frequency responses whose peak frequencies are less precisely captured by the STFT scheme. The spar heave in Fig. 5(g) shows that the good heave performance of the SFOWT system is maintained when the TMDs are installed. Fig. 5(h) presents the spar TMD real-time frequency.



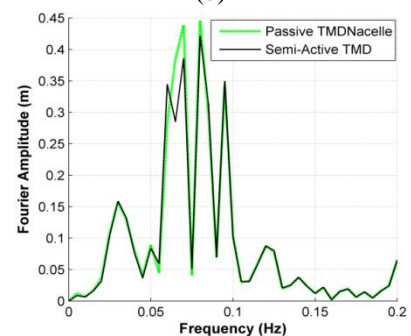
(a)



(b)



(c)



(d)

Continued-

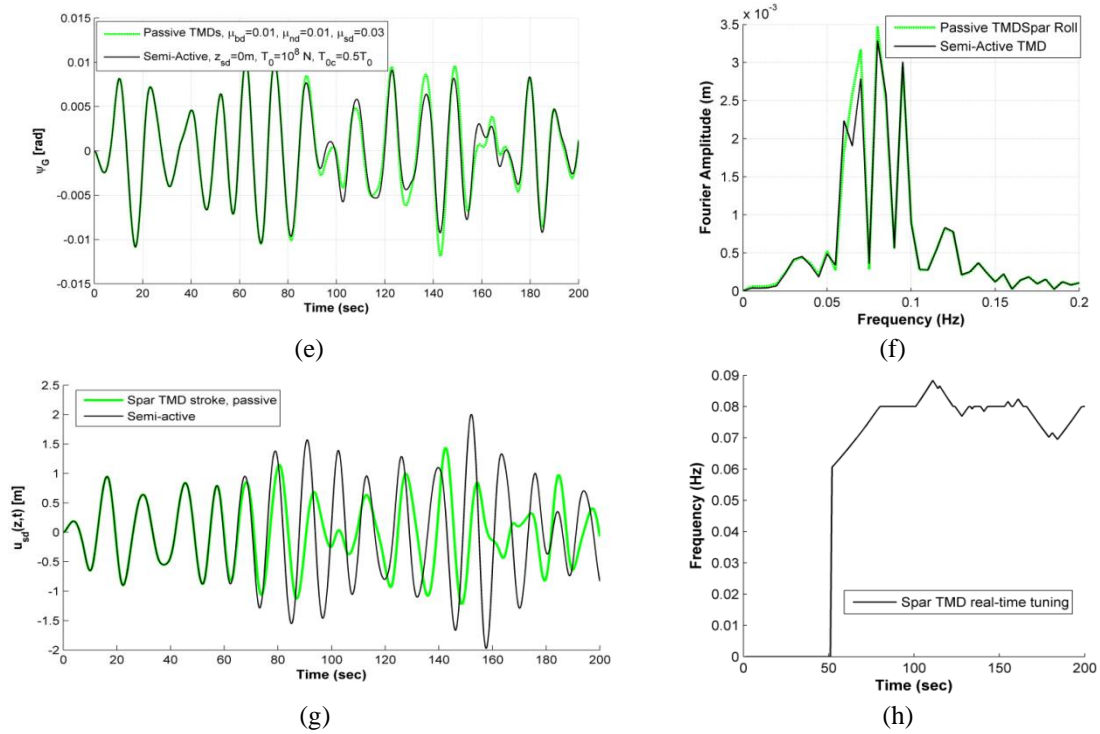
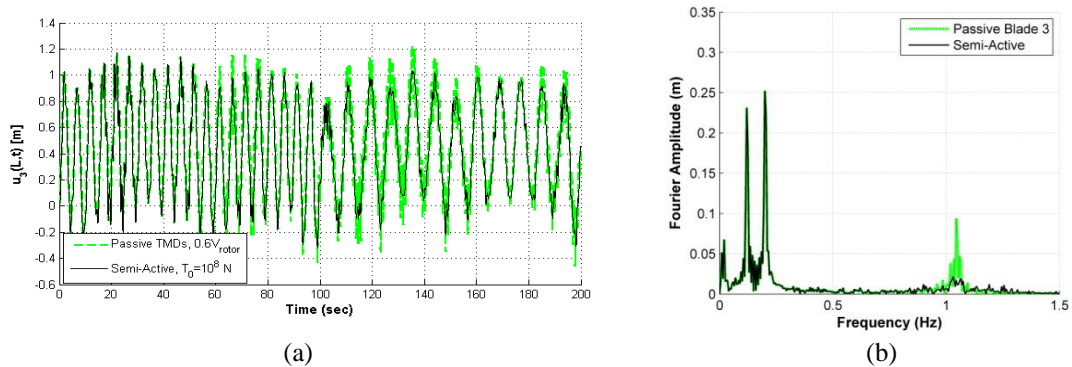


Fig. 5 Responses by passive and semi-active controls, $T_{0c} = 0.5T_0$ at 80 s, (a), (b) Blade; (c), (d) Nacelle sway; (e), (f) Spar roll; (g) Spar TMD stroke; and (h) Spar TMD real-time frequency



Continued-

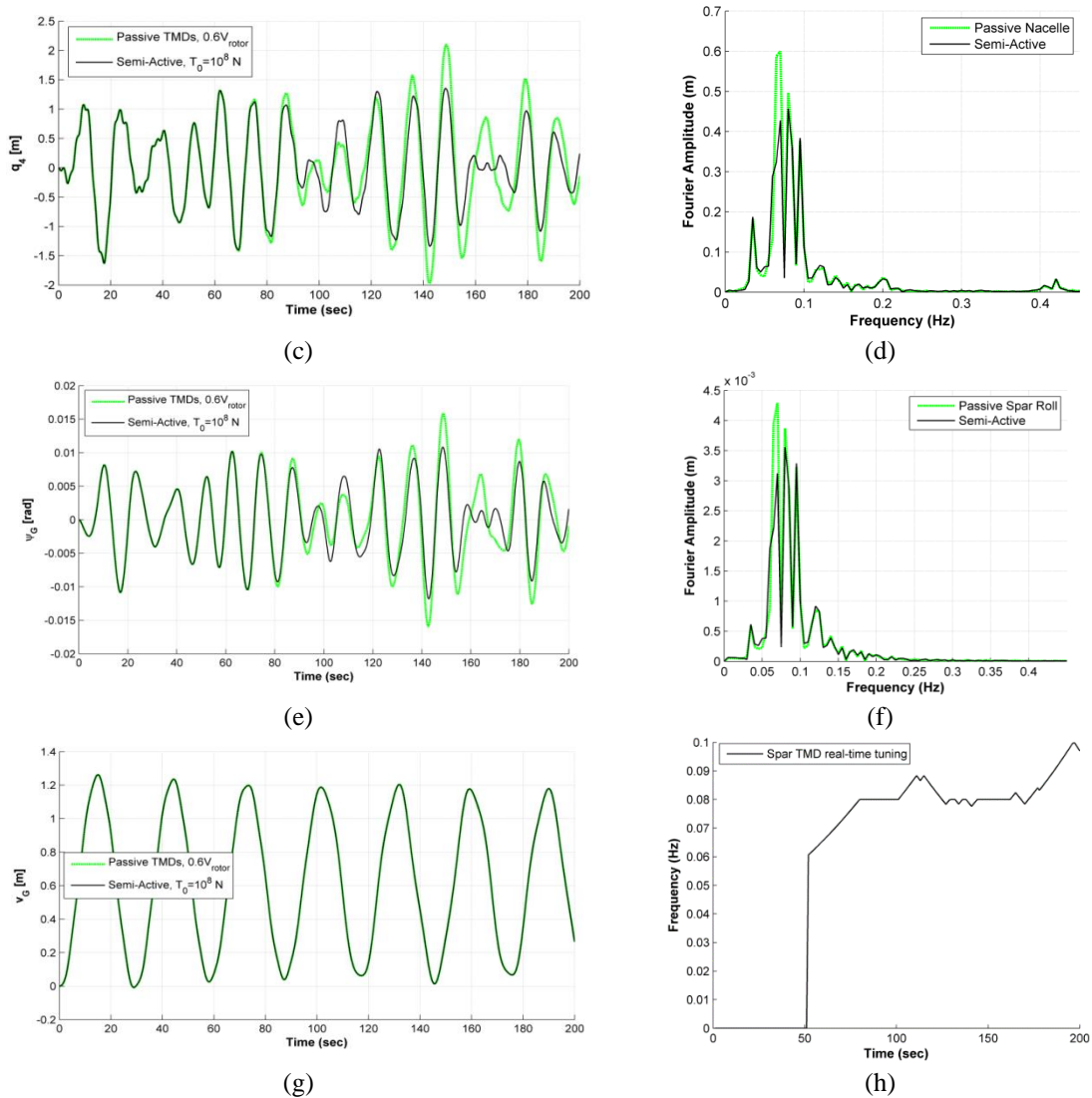


Fig. 6 Responses by passive and semi-active controls, $\Omega_c = 0.6\Omega$ at $t = 100$ s, (a), (b) Blade; (c), (d) Nacelle sway; (e), (f) Spar roll; (g) Spar heave; and (h) Spar TMD real-time frequency

5.3 Varying blade 3 stiffness, mooring cable tension T_0 and rotational speed Ω

This example consider the worst case when the tensions of mooring cable is dropped to $T_{0c} = 0.5T_0$ at a time $t_1 = 80$ s, then the rotor rotational speed is reduced to $\Omega_c = 0.6\Omega$ at a time $t_2 = 100$. Finally the stiffness of blade 3 is lost 50% resulting in a reduction of its fundamental frequency to $\omega_{bc} = 0.7\omega_b$ at a time $t_3 = 120$ s. The time histories and Fourier amplitude spectra of the blade 3 displacement, nacelle sway and spar roll controlled by passive and semi-active TMDs are shown in Figs. 7(a)-7(f), respectively.

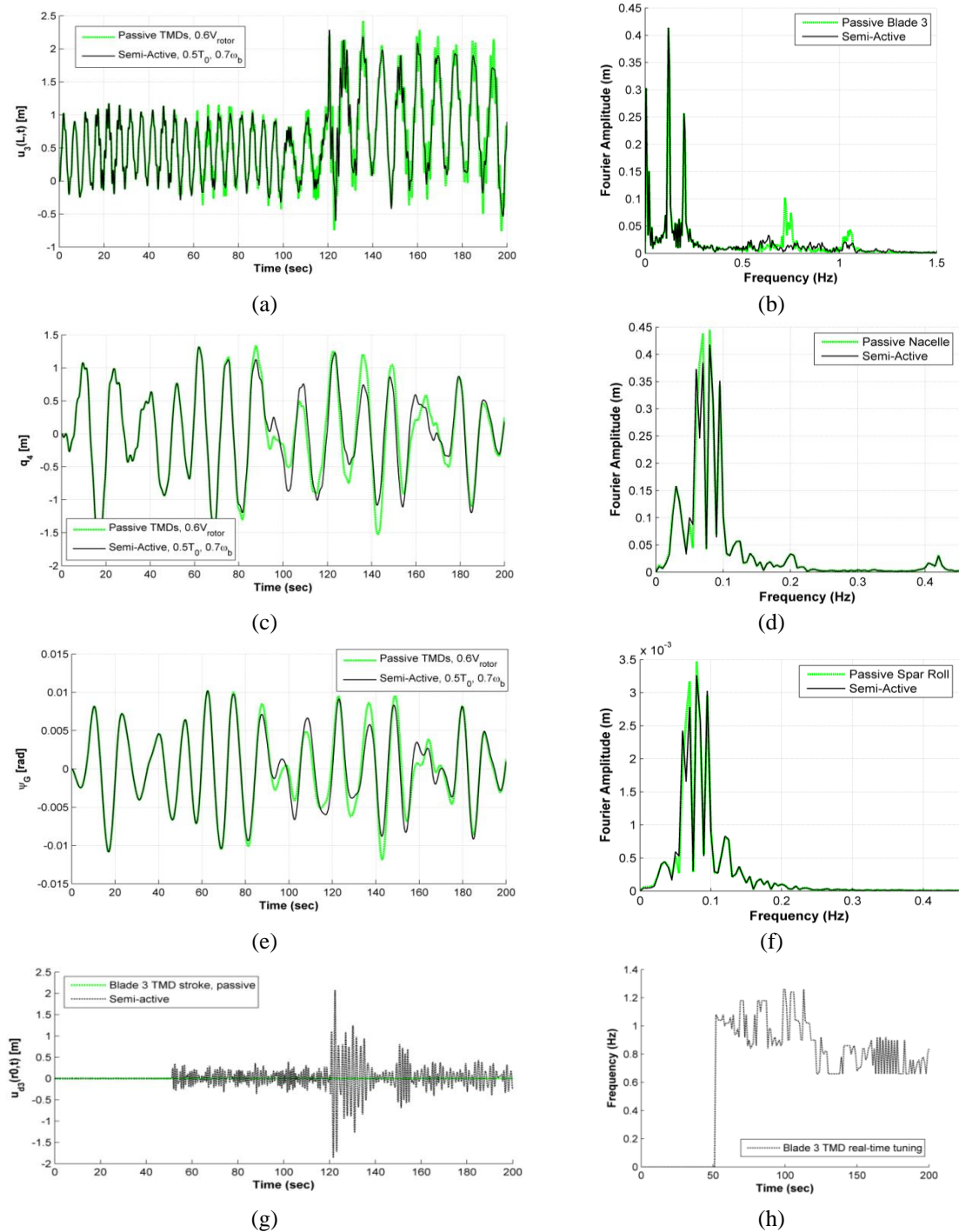


Fig. 7 Responses by passive and semi-active controls, $T_{0c} = 0.5T_0$ at $t_1 = 80$ s, $\Omega_c = 0.6\Omega$ at $t_2 = 100$ s and $\omega_{bc} = 0.7\omega_b$ at $t_3 = 120$ s; (a), (b) Blade; (c), (d) Nacelle sway; (e), (f) Spar roll; (g) Blade 3 TMD stroke; and (h) Blade 3 TMD real-time frequency

The effectiveness of the semi-active control on the blade responses is more profound when the blade stiffness is reduced. This is because that control scheme is capable of tracking the real-time frequencies as shown in Fig. 5(h). However, the effectiveness of the semi-active control on the nacelle sway and spar roll are considerable but less than that of the case of varying rotor speed (in Section 5.2). The blade 3 TMD strokes shown in Fig. 5(g) are acceptable as they are within blade width.

6. Conclusions

In this paper, a TMD has been placed in each blade, in the nacelle and on the spar of spar-type floating wind turbines to control the vibrations at these components. The STFT algorithm has been used for semi-active control of the TMDs. The developed model is a time-varying MDOF system considering the aerodynamic properties of the blade, variable mass and stiffness per unit length, gravity, the interactions among the blades, nacelle, spar, mooring system and the TMDs, the hydrodynamic effects, the restoring moment and the buoyancy force. In the numerical examples, the varying tension of the mooring cables, the varying rotational speed of the blades, and the varying stiffness of a blade have been investigated separately and together. The following conclusions have been drawn:

- Excessive large strokes of nacelle TMD are observed and the instability is occurring when the TMD is tuned at low frequency. The nacelle TMD should be passively controlled and special attention is needed.
- The semi-active control scheme is considerably more effective than passive scheme in all cases. However, the effectiveness is less than as compared to the results for the fixed-base wind turbine cases reported in the literature. This is due to the low-frequency responses whose peak frequencies are less precisely captured by the STFT algorithm.
- The effectiveness of the semi-active control on the blade displacements, nacelle sway and spar roll are larger in the case of varying rotational speed as compared with the case of varying cable tensions.
- The effectiveness of the semi-active control on blade responses is especially profound when the blade stiffness is reduced as the STMD is capable of tracking the real-time frequencies.

Acknowledgements

This research is partly carried out under the EU FP7 funding for the Marie Curie ITN project SYSWIND (Grant No. PITN-GA- 2009-238325). The authors are grateful for the support.

References

- Arrigan, J., Huang, C., Staino, A., Basu, B. and Nagarajaiah, S. (2014), "A frequency tracking semi-active algorithm for control of edgewise vibrations in wind turbine blades", *Smart Struct. Syst.*, **13**(2), 177-201, DOI: 10.12989/sss.2014.13.2.177.
- Arrigan, J., Pakrashi, V., Basu, B. and Nagarajaiah, S. (2011), "Control of flapwise vibration in wind turbine

- blades using semi-active tuned mass dampers”, *Struct. Control Health Monit.*, **18**(8), 840-851, DOI: 10.1002/stc.404.
- Basu, B., Staino, A. and Dinh, V.N. (2012), “Vibration of wind turbines under seismic excitations”, *Proceedings of The 5th Asian-Pacific Symposium on Structural Reliability and its Applications*, Singapore, 439-444, DOI: 10.3850/978-981-07-2219-7_P403.
- Colwell, S. and Basu, B. (2009), “Tuned liquid column dampers in offshore wind turbines for structural control”, *Eng. Struct.*, **31**, 358-368, DOI:10.1016/j.engstruct.2008.09.001.
- Dinh, V.N. and Basu, B. (2012), “Zero-pad effects on conditional simulation and application of spatially-varying earthquake motions”, *Proceedings of The 6th European Workshop on Structural Health Monitoring*, Dresden, Germany, 893-899. URL: www.ndt.net/article/ewshm2012/papers/tu3d3.pdf
- Dinh, V.N. and Basu, B. (2013), “On the modelling of spar-type floating offshore wind turbines”, *Key Eng. Mater.*, **569-570**, 536-543, DOI:10.4028/www.scientific.net/KEM.569-570.636.
- Dinh, V.N. and Basu, B. (2015), “Passive control of floating offshore wind turbine nacelle and spar vibrations by multiple tuned mass damper”, *Struct. Control Health Monit.*, **22**(1), 152-176, DOI: 10.1002/stc.1666.
- Dinh, V.N., Basu, B. and Nielsen, S.R.K. (2013), “Impact of spar-nacelle-blade coupling on the edgewise response of floating offshore wind turbines”, *Coupled Syst. Mech.*, **2**(3), 231-253.
- Faltinsen, O.M. (1990), *Sea Loads on Ships and Offshore Structures*, Cambridge University Press.
- Fitzgerald, B., Basu, B. and Nielsen, S.R.K. (2013), “Active tuned mass dampers for control of inplane vibrations of wind turbine blades”, *Struct. Control Health Monit.*, **20**(12), 1377-1396, DOI: 10.1002/stc.1524.
- Flexcom. www.mcskenny.com/support/flexcom (accessed August 2015).
- Hansen, M.H. (2003), “Improved modal dynamics of wind turbines to avoid stall-induced vibrations”, *Wind Energy*, **6**(2), 179-195, DOI:10.1002/we.79.
- Huang, C., Arrigan, J., Nagarajaiah, S. and Basu, B. (2010), “Semi-active algorithm for edgewise vibration control in floating wind turbine blades”, *Proceedings of the ASCE Earth and Space Conference*, CD ROM, DOI: 10.1061/41096(366)192.
- International Electrotechnical Commission (IEC) (2006), IEC 61400–3, Wind Turbines – Part 3: *Design Requirements for Offshore Wind Turbines*.
- ISSC (2009), Specialist Committee V.4, Ocean wind and wave energy utilization, *17th International Ship and Offshore Structures Congress*, Seoul, Korea.
- Jonkman, J.M. (2010), *Definition of the floating system for Phase IV of OC3*, Technical Report NREL/TP-500-47535, Golden, CO, USA.
- Jonkman, J.M., Butterfield, S., Musial, W. and Scott, G. (2009), *Definition of a 5-MW reference wind turbine for offshore system development*, Technical Report NREL/TP-500-38060, USA.
- Lackner, M.A. (2009), “Controlling platform motions and reducing blade loads for floating wind turbines”, *Wind Eng.*, **33**(6), 541-553.
- Lackner, M.A. and Rotea, M.A. (2011), “Structural control of floating wind turbines”, *Mechatronics*, **21**, 704-719, DOI:10.1016/j.mechatronics.2010.11.007.
- MATLAB, The MathWorks, Inc., Natick, United States. Release 2011b.
- Murtagh, P.J., Ghosh, A., Basu, B. and Broderick, B.M. (2008), “Passive control of wind turbines vibrations including blade/tower interaction and rotationally sampled turbulence”, *Wind Energy*, **11**(4), 305-317.
- Nagarajaiah, S. (2009), “Adaptive passive, semiactive, smart tuned mass dampers: identification and control using empirical mode decomposition, Hilbert transform, and short-term Fourier transform”, *Struct. Control Health Monit.*, **16**(7-8), 800-841, DOI: 10.1002/stc.349.
- Nagarajaiah, S. and Sonmez, E. (2007), “Structures with semiactive variable stiffness single/multiple tuned mass dampers”, *J. Struct. Eng. - ASCE*, **133**(1), 67-77.
- Nagarajaiah, S. and Varadarajan, N. (2005), “Short time Fourier transform algorithm for wind response control of buildings with variable stiffness TMD”, *Eng. Struct.*, **27**, 431-441.
- Sannasiraj, S.A., Sundar, V. and Sundaravadivelu, R. (1998), “Mooring forces and motion responses of pontoon-type floating breakwaters”, *Ocean Eng.*, **25**(1), 27-48.

- Sarpkaya, T. and Isaacson, M. (1981), *Mechanics of Wave Forces on Offshore Structures*, Van Nostrand Reinhold, New York.
- Staino, B., Basu, B. and Nielsen, S.R.K. (2012), "Actuator control of edgewise vibrations in wind turbine blades", *J. Sound Vib.*, **331**, 1233-1256, DOI:10.1016/j.jsv.2011.11.003.
- Waris, M.B. and Ishihara, T. (2012), "Dynamic response analysis of floating offshore wind turbine with different types of heave plates and mooring systems by using a fully nonlinear model", *Coupled Syst. Mech.*, **1**(3), 247-268.

BS

Appendix A

Mass matrix:

$$\mathbf{M} = \begin{bmatrix} m_{2d} & \hat{m}_d & 0 & 0 & 0 & 0 & -m_{11}^d & -m_{11}^d & -\bar{m}_{11}^d & h_a m_{11}^d & 0 & 0 \\ \hat{m}_d & m_d & 0 & 0 & 0 & 0 & -m_{d1} & -m_{d1} & -\bar{m}_{d1} & h_a m_{d1} & 0 & 0 \\ 0 & 0 & m_{2d} & \hat{m}_d & 0 & 0 & -m_{12}^d & -m_{12}^d & -\bar{m}_{12}^d & h_a m_{12}^d & 0 & 0 \\ 0 & 0 & \hat{m}_d & m_d & 0 & 0 & -m_{d2} & -m_{d2} & -\bar{m}_{d2} & h_a m_{d2} & 0 & 0 \\ 0 & 0 & 0 & 0 & m_{2d} & \hat{m}_d & -m_{13}^d & -m_{13}^d & -\bar{m}_{13}^d & h_a m_{13}^d & 0 & 0 \\ 0 & 0 & 0 & 0 & \hat{m}_d & m_d & -m_{d3} & -m_{d3} & -\bar{m}_{d3} & h_a m_{d3} & 0 & 0 \\ -m_{11}^d & -m_{d1} & -m_{12}^d & -m_{d2} & -m_{13}^d & -m_{d3} & m_{4nd} & m_{4nd} & 0 & -h_a m_{4nd} & m_{nd} & 0 \\ -m_{11}^d & -m_{d1} & -m_{12}^d & -m_{d2} & -m_{13}^d & -m_{d3} & m_{4nd} & m_{4nsd} & 0 & -I_{\varphi u} & m_{nd} & m_{sd} \\ -\bar{m}_{11}^d & -\bar{m}_{d1} & -\bar{m}_{12}^d & -\bar{m}_{d2} & -\bar{m}_{13}^d & -\bar{m}_{d3} & 0 & 0 & m_{4sd} & 0 & 0 & 0 \\ h_a m_{11}^d & h_a m_{d1} & h_a m_{12}^d & h_a m_{d2} & h_a m_{13}^d & h_a m_{d3} & -h_a m_{4nd} & -I_{\varphi u} & 0 & m_{\varphi\varphi}^d & 0 & 0 \\ 0 & 0 & 0 & 0 & 0 & 0 & m_{nd} & m_{nd} & 0 & 0 & m_{nd} & 0 \\ 0 & 0 & 0 & 0 & 0 & 0 & 0 & m_{sd} & 0 & 0 & 0 & m_{sd} \end{bmatrix} \quad (\text{A1})$$

where

$$m_1 = \int_0^R \mu(r) \phi_1 dr; \quad m_2 = \int_0^R \mu(r) \phi_1^2 dr; \quad m_4 = 3 \int_0^R \mu(r) dr + M_0 \quad (\text{A2})$$

$$m_{1i} = m_1 \cos \psi_i; \quad \bar{m}_{1i} = m_1 \sin \psi_i \quad (\text{A3})$$

$$\hat{m}_d = m_d \phi_1(r_0); \quad \bar{m}_d = m_d \phi_1^2(r_0); \quad m_{2d} = m_2 + \bar{m}_d \quad (\text{A4})$$

$$m_{1i}^d = m_{1i} + m_d \phi_1(r_0) \cos \psi_i = [m_1 + m_d \phi_1(r_0)] \cos \psi_i; \quad m_{di} = m_d \cos \psi_i \quad (\text{A5})$$

$$\bar{m}_{1i}^d = \bar{m}_{1i} + m_d \phi_1(r_0) \sin \psi_i = [m_1 + m_d \phi_1(r_0)] \sin \psi_i; \quad \bar{m}_{di} = m_d \sin \psi_i \quad (\text{A6})$$

$$m_{4nd} = m_4 + 3m_d + m_{nd}; \quad m_{4nsd} = m_{4nd} + M_s + m_{sd}; \quad m_{4sd} = m_4 + M_s + 3m_d \quad (\text{A7})$$

$$m_{\varphi\varphi} = I_s + h_a^2 m_4; \quad m_{\varphi\varphi}^d = m_{\varphi\varphi} + h_a^2 (3m_d + m_{nd}) + (z + h_G)^2 m_{sd} \quad (\text{A8})$$

$$m_{\varphi u} = h_a (3m_d + m_{nd}) + (z + h_G) m_{sd}; \quad I_{\varphi u} = h_a m_4 + m_{\varphi u} \quad (\text{A9})$$

where

$$k_{bi} = k_2 + K_w \cos \psi_i; \quad k_2 = K_e + \Omega^2 K_g - \Omega^2 m_2 \quad (\text{A12})$$

$$k_{bd} = m_d \Omega^2 \phi_1(r_0); \quad \bar{k}_{bd} = m_d \Omega^2 \phi_1^2(r_0); \quad (\text{A13})$$

$$k_{ts} = k_t + k_{sH}; \quad k_{t\phi} = -h_d k_t \quad (\text{A14})$$

The horizontal, vertical and rolling stiffness of the mooring system in the stiffness matrix, are obtained from the extended quasi-static model of mooring cable (Sannasiraj *et al.* 1998) and are respectively expressed as

$$k_{sH} = \frac{w}{T_0} \left(\frac{L'T_C - lT_F}{T_F - T_C} \right) k_{HV} \quad (\text{A15})$$

$$k_{sV} = \frac{w}{T_0} \left(\frac{T_F T_C}{T_F - T_C} \right) \left[\frac{Y_{FC}}{T_0} - \left(\frac{L'T_C - lT_F}{T_F T_C} \right) \right] k_{HV} \quad (\text{A16})$$

$$k_{s\phi} = \left\{ \begin{array}{l} \frac{w(z_F - z_G)^2}{T_0} \left(\frac{L'T_C - lT_F}{T_F - T_C} \right) + \frac{w(y_G - y_F)^2}{T_0} \left(\frac{T_F T_C}{T_F - T_C} \right) \left[\frac{Y_{FC}}{T_0} - \left(\frac{L'T_C - lT_F}{T_F T_C} \right) \right] \\ + 2(y_G - y_F)(z_F - z_G) \end{array} \right\} k_{HV} \quad (\text{A17})$$

where

$$k_{HV} = T_0 \left\{ w \left(\frac{L'T_C - lT_F}{T_F - T_C} \right) \left[\frac{Y_{FC}}{T_0} - \left(\frac{L'T_C - lT_F}{T_F T_C} \right) \right] - \frac{T_0^2 Z_{FC}}{T_F T_C} \right\}^{-1} \quad (\text{A18})$$